Peculiar Rashba spin texture induced by C_{3v} symmetry on the Bi(111) surface revisited

Koji Miyamoto,[1,*] Hirokazu Miyahara,[2] Kenta Kuroda,[2,3] Takamasa Maegawa,[2] Akio Kimura,[2] and Taichi Okuda[1,†]

[1]*Hiroshima Synchrotron Radiation Center, Hiroshima University, Higashi-Hiroshima 739-0046, Japan*

[2]*Graduate School of Science, Hiroshima University, Higashi-Hiroshima 739-8526, Japan*

[3]*Institute for Solid State Physics, University of Tokyo, Kashiwa, Chiba 277-8581, Japan*

(Received 5 December 2017; published 23 February 2018)

The spin texture of the spin-split surface states on Bi(111) has been comprehensively investigated by high energy and angular resolution spin- and angle-resolved photoelectron spectroscopy. A large out-of-plane spin component that alternately changes its sign is clearly observed. There is no evidence for peculiar polarization oscillation of the in-plane spin component, which was suggested to be due to breaking of the time-reversal symmetry in a previous report [A. Takayama *et al.*, Phys. Rev. Lett. **106**, 166401 (2011)]. The observed band structure and spin polarization are well reproduced by the kp model Hamiltonian considering the C_{3v} crystal symmetry, and the in-plane polarization variation at the different k points can be understood by the photoemission final-state effect.

DOI: 10.1103/PhysRevB.97.085433

I. INTRODUCTION

Bismuth has been extensively studied because of its peculiar physical properties, such as its large bulk Fermi wavelength, large bulk resistivity, and hole coefficient, which are related to its semimetallicity [1,2]. Because of its large atomic number, Bi also possesses a large spin-orbit interaction (SOI), and it has recently attracted much attention as the major element of topological insulators or materials showing large Rashba spin splitting. For instance, a substantial Rashba spin splitting is observed in the surface states of the $BiAg_2$ alloy [3], Bi/Si(111) [4], and Bi/Ge(111) [5]. Spin-orbit coupling could cause the bulk band inversion that results in the topological insulator phase as actually found in Bi_xSb_{1-x} [6,7], Bi_2Se_3 [8–10], and some ternary compounds [11–15] accompanying the topologically protected spin-split surface states.

Even the simple Bi metal is known to exhibit large surface Rashba spin splitting [16,17]. Energy dispersion of the Bi(111) surface has been investigated by angle-resolved photoelectron spectroscopy (ARPES) [16], and the observed characteristic dispersion has been relatively well reproduced by the first-principles calculations [17]. The two metallic surface states S_1 and S_2 are ascribed to Rashba spin-split surface states forming electron and hole pockets in the Fermi surfaces (FSs) [16]. Direct evidence for Rashba spin splitting has been obtained by spin-resolved ARPES (SARPES) measurements [18,19]. In measurements of in-plane spin polarization perpendicular to the electron wave vector and the potential gradient (i.e., surface normal), reversal of the spin polarization against the time-reversal-invariant momentum $\bar{\Gamma}$ is clearly observed. Interestingly, these surface states are similar to those of Bi_xSb_{1-x} [6] in terms of the band structure features and FS shapes. Recently, there has also been a dispute about whether the topological nature of Bi(111) is topologically trivial or nontrivial [20–22]. Thus, Bi(111) has recently attracted much attention.

By independent SARPES observation, Takayama *et al.* [23] found that the S_2 state contains a considerable out-of-plane spin component at the $\bar{K}$ point that deviates from the Rashba spin splitting of the ideal two-dimensional electron gas. They found that the sign of the out-of-plane spin polarization alternately changes at every adjacent $\bar{K}$ point. The degree of in-plane spin polarization also oscillates at every adjacent $\bar{K}$ point, and the magnitude is not completely reversed at opposite momentum. Moreover, they suggested that the magnitude of spin polarization is not affected by the experimental geometry. Thus, they claimed that the time-reversal symmetry is broken in the initial state of Bi(111). However, the observed SARPES spectra in their study were averaged in large **k** space, resulting in a featureless spectral shape and the degree of spin polarization being obscured, probably because of the limited angular resolution in the spin detection with the Mott-type spin polarimeter of Ref. [23]. In addition, the intrinsic low efficiency of the SARPES observation limits the number of measurement points in **k** space, which makes data interpretation very speculative.

In this study, we revisited the Bi(111) surface and performed the comprehensive SARPES observations with high energy and angular resolutions using our SARPES system [24,25]. The 100 times higher efficiency of the very low energy electron diffraction (VLEED) spin polarimeter compared with conventional spin detectors allows SARPES measurements with high energy and angular resolutions ($\Delta E \sim 20$ meV, $\Delta k \sim \pm 0.02$ Å^{-1}), which enables the characteristic spin texture of the surface states of Bi(111) with numerous k points to be revealed. As a consequence, the out-of-plane spin component with a high degree of spin polarization is clearly observed in the S_2 state. In addition to the S_2 state, in the S_1 state, an out-of-plane spin-polarization component and an in-plane spin-polarization are observed. In addition, there is the evidence that the in-plane spin-polarization oscillation of the S_2 state in the initial state as reported in Ref. [26] doesn't occur. The observed band and spin structures are well reproduced by an effective Hamiltonian based on the kp perturbation theory considering the C_{3v} crystal symmetry. These findings strongly suggest

*kmiyamoto@hioshima-u.ac.jp
†okudat@hioshima-u.ac.jp

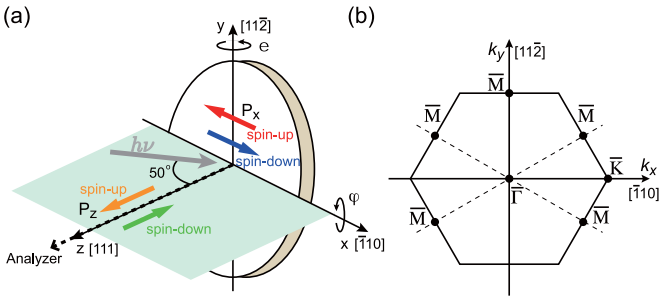

FIG. 1. (a) Experimental geometry of the SARPES measurement and the definition of spin polarization. (b) Surface Brillouin zone of Bi(111).

that the previously reported spin-polarization variation in the in-plane spin component of the S_2 state at the different k points is probably because of the photoemission final-state effect.

II. EXPERIMENT

The Bi(111) single-crystal film was grown at room temperature by Bi evaporation from a Knudsen cell on the Si(111) 7 × 7 surface which was obtained by direct current heating up to 1500 K [27]. After evaporation of Bi, the sample was annealed at 400 K for 30 min to obtain a well-ordered single-crystal film with large terrace width [28]. The quality of the film was confirmed by the sharp 1 × 1 diffraction spots of low-energy electron diffraction (LEED), the clear surface states of the ARPES spectra, and the absence of the peaks of contaminants in the Auger electron spectrum.

The ARPES and SARPES measurements were performed at the sample temperature of 80 K with a HeI_α discharge lamp ($h\nu = 21.22$ eV) using the high-resolution SARPES apparatus (Efficient SPin REsolved SpectroScopy Observation: ESPRESSO) [25] installed at beamline BL-9B in the Hiroshima Synchrotron Radiation Center (HSRC). The energy and angular resolutions were set to $\Delta E \sim 10$ meV and $\Delta\theta \sim 0.1^\circ$ for ARPES and $\Delta E \sim 20$ meV and $\Delta\theta \sim \pm 0.35^\circ$ for SARPES. As shown in Fig. 1(a), the angle between the light incidence and the electron analyzer is fixed at 50°. The spin components of both the x and z directions can be observed in the spin-detector coordinate system, which correspond to the in-plane (P_x) and out-of-plane (P_z) spin components of the observed sample at normal emission. Note that the coordinates of the spin detector and sample can be distinguished when the sample is set for off-normal emission. The small tilt ($|\varphi| < 4^\circ$) and polar ($|\theta| < 4^\circ$) angles in the present measurement, however, ensure that the difference between the original spin polarization in the sample coordinate system and the projected spin component onto the spin-detector coordinate system is negligible (less than 0.3%).

III. RESULTS and DISCUSSION

Figures 2(a)–2(c) show the spin-integrated energy-momentum (E-k) frames along the $\bar{\Gamma}$-$\bar{K}$ and $\bar{\Gamma}$-$\bar{M}$ lines [see Fig. 1(b)] and the FS of the Bi(111) film, respectively. The surface states S_1 and S_2 are clearly observed. The observed dispersion and FS features of the surface states are in good agreement with previous reports [16,17]. Namely, the band structure of S_1 and S_2 yields a hexagonal electron pocket at around $\bar{\Gamma}$ and the petal-like hole pocket along the $\bar{\Gamma}$-$\bar{M}$ line at the Fermi level [top panel in Fig. 2(c)]. The petal-like hole pocket rises with increasing binding energy E_B and evolves into a wedge structure at $E_B \sim 100$ meV, as shown in the bottom panel of Fig. 2(c). In contrast, the hexagonal electron pocket shrinks with increasing E_B and almost disappears at $E_B \sim 100$ meV. The characteristic band dispersion and evolution of the constant energy contours (CECs) of the surface states of Bi(111) are in contrast to the isotropic electronic structure of the free-electron-like surface states of Au(111) [29], even though they are both Rashba spin-split surface states. The features of the band dispersions and CECs resemble those of $Bi_{1-x}Sb_x$, a three-dimensional topological insulator, suggesting the commonality between the two [6]. This similarity originates from the electronic structure of the Bi crystal governed by the strong SOI with C_{3v} crystal symmetry. It is concluded that the spin texture of systems with a strong SOI and C_{3v} crystal symmetry, such as Bi_2Te_3 and the $BiAg_2$ surface alloy, shows significant out-of-plane spin polarization at the $\bar{\Gamma}$-$\bar{K}$ line of the so-called warped FS of the spin-split surface states [3,30], which has been directly observed by SARPES measurements [31,32].

To investigate the anisotropic electronic structures and spin structures of S_1 and S_2, we attempted to reproduce the observed electronic band dispersion using a model Hamiltonian based on the third-order kp perturbation theory with surface symmetry [33–36]. For C_{3v} symmetry, the model Hamiltonian is expressed as

$$H = \frac{\hbar^2 k^2}{2m^*} + \alpha_k(k_x\sigma_y - k_y\sigma_x) + \frac{\lambda}{2}(k_+^3 + k_-^3)\sigma_z, \quad (1)$$

where $k_\pm = k_x \pm ik_y$; $\alpha_k = \alpha_R(1 + ck^2)$; and m^*, α_R, and λ are the electron effective mass, the so-called Rashba parameter, and warping parameter, respectively. From the Hamiltonian, the energy eigenvalue of Eq. (1) can be expressed as

$$E = \frac{\hbar^2 k^2}{2m^*} \pm \sqrt{\alpha_k^2 k^2 + \lambda^2 k^6 cos^2(3\phi)}. \quad (2)$$

The plus and minus signs in the eigenvalue correspond to the calculated spin components for the S_1 and S_2 states, respectively. Here, ϕ is defined as an azimuthal angle, as shown in Fig. 2(c).

The spin polarizations P_x, P_y, and P_z can be calculated by

$$P_x = \frac{2\alpha_k k_y}{N}[d_\pm - \lambda k^3 \cos(3\phi)], \quad (3)$$

$$P_y = -\frac{2\alpha_k k_x}{N}[d_\pm - \lambda k^3 \cos(3\phi)], \quad (4)$$

$$P_z = \frac{2\lambda k^3 \cos(3\theta)}{N}[d_\pm - \lambda k^3 \cos(3\phi)], \quad (5)$$

where

$$d_\pm = \pm\sqrt{\alpha_k^2 k^2 + \lambda^2 k^6 \cos^2(3\phi)},$$

$$N = \alpha_k^2 k^2 + [-d_\pm - \lambda k^3 \cos(3\phi)]^2.$$

First, we fitted the ARPES results along $\bar{\Gamma}$-$\bar{M}$ to obtain all of the parameters except for λ. The final fitting parameter λ was determined by fitting the ARPES results along $\bar{\Gamma}$-$\bar{K}$. All of

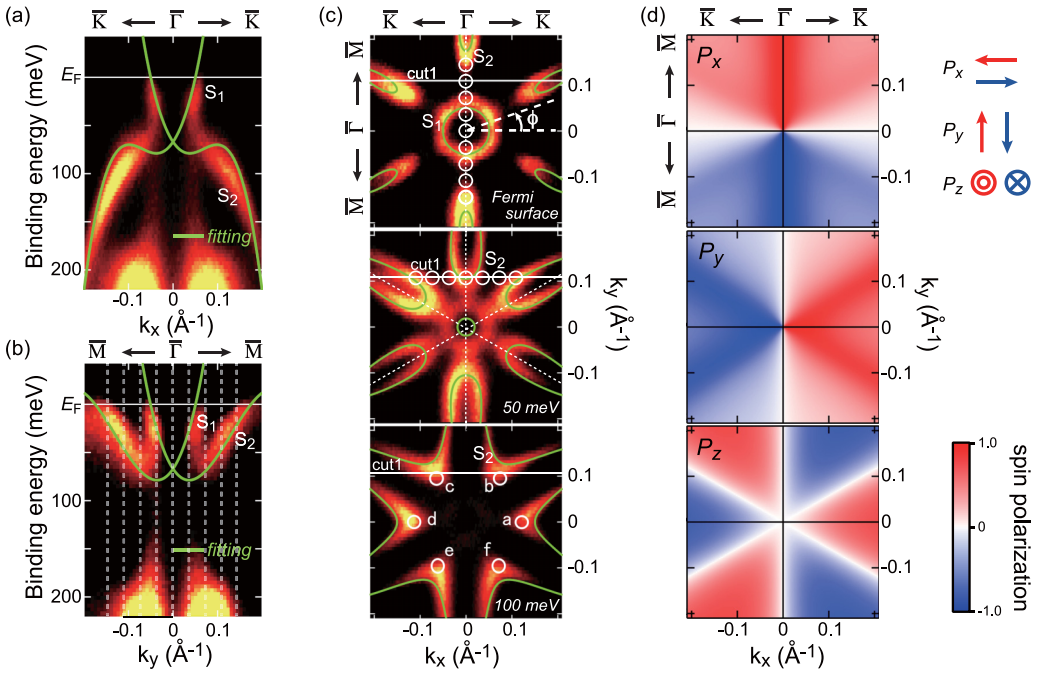

FIG. 2. Band dispersion of the surface states along the (a) $\bar{\Gamma}$-$\bar{K}$ and (b) $\bar{\Gamma}$-$\bar{M}$ directions obtained by the spin-integrated ARPES measurements. Here, vertical dashed lines show the k_y points that correspond to the measured emission angles in Fig. 3. (c) Evolution of the constant-energy contour (CEC) of the bands taken at the Fermi energy E_F, $E_B = 50$ and 100 meV. The green solid curves are fitting results of the band dispersion as well as the constant energy calculated with Eq. (1) (see text). White open circles in the top, middle, and bottom panels represent k points corresponding to the measured emission angle of the spin-ARPES experiment in Figs. 3, 4, and 5, respectively. In the middle panel, the dashed lines show $\bar{\Gamma}$-$\bar{M}$ lines. (d) Spin polarization (P_x, P_y, P_z components) of the S_2 state in k space calculated with the fitting parameters obtained by the fitting procedure.

the fitting parameters are summarized in Table I. The fitting results are shown as green solid curves in Figs. 2(a)–2(c). The experimental band dispersion and CEC are well reproduced with the model Hamiltonian.

The calculated spin polarizations for the P_x, P_y, and P_z components of the S_2 state are plotted as functions of the wave vectors k_x and k_y in Fig. 2(d). The spin polarization is represented by the red-white-blue color code, where red (blue) represents the positive (negative) values. The directions of the spin polarization of P_x, P_y, and P_z are defined in the inset of Fig. 2(d). The sign reversal of the calculated spin polarization of the out-of-plane spin component P_z clearly indicates the $2\pi/3$ periodicity of the polarization sign reversal. The in-plane spin component shows approximately 2π periodicity, which is consistent with the ordinary Rashba spin splitting and represents the counterclockwise helical spin texture.

TABLE I. Parameters obtained by fitting the band dispersion of the Bi(111) surface states using the model Hamiltonian. m^*, α_R, λ, and c are the electron effective mass, the Rashba parameter, the warping parameter, and the parameter indicating the contribution of the k^3 term, respectively.

	Parameter			
Material	m^* (m_e)	α_R (eVÅ)	c (eVÅ^2)	λ (eVÅ^3)
Bi(111)	0.34	0.70	41	60

Figure 3 shows the in-plane spin-resolved energy distribution curves (EDCs) along the $\bar{\Gamma}$-$\bar{M}$ direction, which which correspond to the ARPES result in Fig. 2(b). Here, spin-up and spin-down states are shown with triangles pointing up and down, respectively. The peak positions of the S_1 and S_2 states and their upward dispersion along the $\bar{\Gamma}$-$\bar{M}$ direction are well resolved. Spin-polarization reversal against the $\bar{\Gamma}$ point ($\theta = 0^\circ$) is also clearly observed in both the S_1 and S_2 states, which is in good agreement with Rashba spin splitting. Note that the degree of spin polarization is much higher than that of previous reports using a conventional SARPES apparatus [18,19], which is probably because of the higher energy and angular resolution of the present measurements. Furthermore, the magnitude of spin polarization ($|P| = 90\%$) in the S_2 state at positive θ is a bit larger than that ($|P| = 75\%$) at negative θ. This difference of the spin polarization is probably due to the final-state effect, as indicated in the following section.

Unlike the ideal Rashba spin-split states that have only in-plane spin polarization, the existence of the out-of-plane spin component is suggested in the S_2 state [23]. According to Ref. [23], the sign of the out-of-plane spin component P_z changes with respect to the $\bar{\Gamma}$-$\bar{M}$ line, as in the bottom panel of Fig. 2(d), where the alternate sign change of the P_z spin component is shown with the red-white-blue color code. As shown in Fig. 2(c), the petal-shaped FS of the S_2 states approaches the $\bar{\Gamma}$-$\bar{K}$ line with increasing E_B and evolves into a wedge shape at $E_B = 100$ meV. Thus, the out-of-plane spin component will be observed at the cusp of the wedge structure at E_B, if it exists. To investigate the proposed peculiar spin

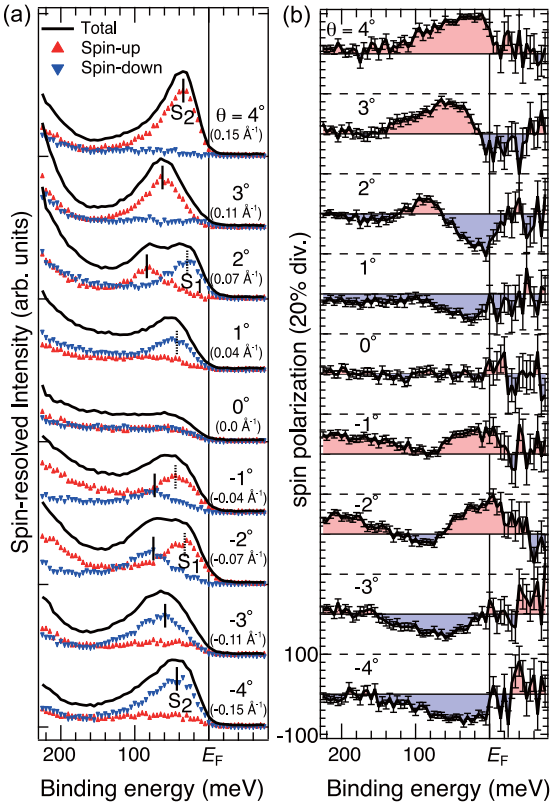

FIG. 3. (a) Spin- and angle-resolved photoelectron spectra and (b) the corresponding spin polarization of the surface states of Bi(111) along the $\bar{\Gamma}$-$\bar{M}$ direction, which corresponds to the band mapping in Fig. 2(b). The wave numbers corresponding to the measured angles at Fermi energy are given in parentheses. Triangles pointing up and down in the SARPES spectra correspond to spin-up and spin-down states, respectively. The dashed and solid lines represent the peak positions corresponding to S_1 and S_2 states, respectively. Because of the high energy and angular resolution, the observed degree of spin polarization is much higher than in previous studies and the two spin-split surface states (S_1 and S_2) are clearly resolved in the SARPES spectra.

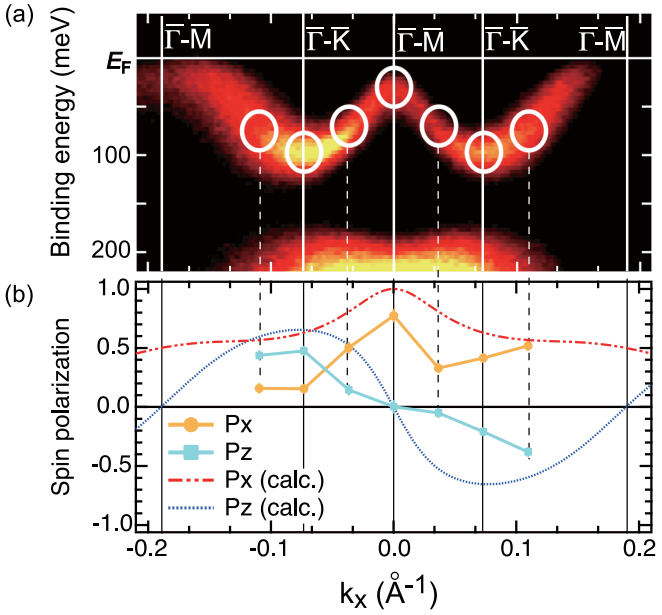

FIG. 4. (a) Band dispersion of the S_2 state along the line (cut 1) indicated in Fig. 2(c). (b) Spin polarization of the in-plane (P_x; circles) and out-of-plane (P_z; squares) spin components obtained at the k points indicated by the white circles in (a). The sizes of the circles in (a) represent the angular resolution of the measurements. The long- and short- dashed red curve (dashed blue line) indicates the calculated out-of-plane (in-plane) spin polarization utilizing the kp model Hamiltonian. Vertical solid lines show the wave numbers where the line cut 1 and $\bar{\Gamma}$-$\bar{M}$ ($\bar{\Gamma}$-$\bar{K}$) line intersect each other.

texture of the S_2 state [23], we measured both the in-plane and out-of-plane spin polarization of the S_2 state at the cusp positions at $E_B = 100$ meV. Note that only the S_2 state can be detected, as shown in Figs. 2(a) and 2(b).

To investigate the $\boldsymbol{k}$ dependence of the out-of-plane spin polarization, we observed the spin-resolved EDCs at several k points along the line (cut 1) indicated in Fig. 2(c). The cut 1 line crosses three $\bar{\Gamma}$-$\bar{M}$ lines and two $\bar{\Gamma}$-$\bar{K}$ lines in first surface Brillouin zone, as shown by vertical lines in Fig. 4. As shown in Fig. 4(a), the S_2 state shows upward dispersion from the cusp position ($\bar{\Gamma}$-$\bar{K}$ line) toward the $\bar{\Gamma}$-$\bar{M}$ line. The observed spin polarization at the points indicated by white circles in Fig. 4(a) is plotted in Fig. 4(b). There is a clear sign reversal of the out-of-plane spin polarization with respect to the $\bar{\Gamma}$-$\bar{M}$ line ($k_x = 0.0$Å^{-1}). Since the sign of the out-of-plane spin polarization is opposite for adjacent wedge structures, the spin polarization is expected to disappear at the $\bar{\Gamma}$-$\bar{M}$ line, and this disappearance of the spin polarization at the $\bar{\Gamma}$-$\bar{M}$ line is actually observed. Note that this is also natural because the $\bar{\Gamma}$-$\bar{M}$ line is placed in a vertical mirror plane and the P_z component should be zero by considering the symmetry. In addition, the observed $\boldsymbol{k}$ dependence of P_x and P_z spin polarization along the line (cut 1) in Fig. 4(b) is reproduced by the spin feature calculated by the model Hamiltonian [red curve in Fig. 4(b)], except for the magnitude of the spin polarization. The discrepancy of the magnitude of the spin polarization will be discussed later.

Here, let us note the spin-resolved EDC of the cusp positions labeled a–f in Fig. 2(c), as indicated in Fig. 5. In the experimental setup, the out-of-plane and in-plane spin components correspond to spin polarization normal (P_z) and parallel (P_x) to the surface of the emission plane. As a result, significant out-of-plane spin components are observed in Fig. 5(a). In Fig. 5(a), the dominant spin component is up at points a, c, and e, while it is down at points b, d, and f. That is, the sign of the observed out-of-plane spin polarization is opposite between adjacent cusp positions (i.e., the $\bar{\Gamma}$-$\bar{K}$ line).

In contrast to the peculiar spin-polarization behavior of the out-of-plane spin component, the $\boldsymbol{k}$ dependence of the in-plane spin component approximately follows the ordinary Rashba spin-split state of the ideal two-dimensional electron gas [see Fig. 6(b)]. That is, at points b and c, which are in the upper half of the surface Brillouin zone (SBZ), the in-plane (P_x) spin polarization is positive, while it is reversed at points e and f, which are in the lower half of the SBZ. This sign reversal of the in-plane spin component is consistent with the counterclockwise tangential spin polarization observed in a previous study [19] and the calculated spin feature in Fig. 2(d).

In order to understand the k-position dependence of the spin polarization, the observed in-plane and out-of-plane spin-

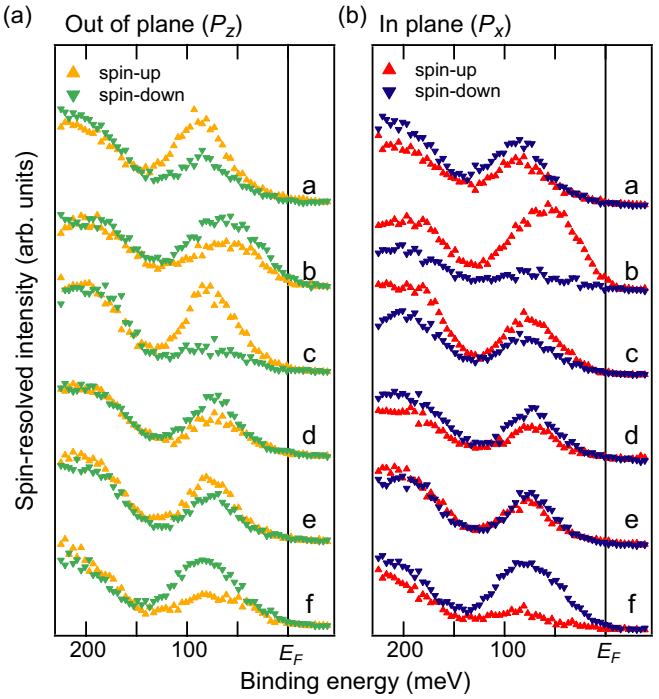

FIG. 5. Spin- and angle-resolved photoelectron spectra at points a–f in Fig. 2(c). In both the (a) out-of-plane spin and (b) in-plane spin spectra, spin-up and spin-down states are shown as upward- and downward-pointing triangles, respectively.

polarization values are plotted as a function of the azimuth angle ϕ from the dashed line ($\bar{\Gamma}$-$\bar{K}$ line), which is defined as in Fig. 2(c), in Fig. 6(a). Note that the behavior of the in-plane spin polarization deviates from the spin feature estimated by our model Hamiltonian considering the crystal symmetry, as shown by the red solid line in Fig. 6(c). Namely, although the magnitude of the spin polarization is equal between points b and c or e and f in the model calculation, the observed values at points b and f are larger than those at points c and e in the experiment. Furthermore, negative spin polarization is observed at points a and d, where the spin polarization is expected to be zero, as shown in the model Hamiltonian [see Fig. 2(d)].

The results may remind us of the scenario of time-reversal symmetry breaking in the S_2 states of Bi(111) proposed by Takayama *et al.*, which suggest that the magnitude of in-plane spin polarization is also modulated with $2\pi/3$ periodicity [23] [see inset of Fig. 6(a)]. However, in their study, the scenario is simply deduced without clear evidence from the spin-polarization difference between a pair of opposed k points against the $\bar{\Gamma}$ point. Because the spin polarization can be affected by the photoemission final-state effect [26], care should be taken when verifying the scenario from the limited data points.

In order to investigate the scenario of time-reversal symmetry breaking of the initial state, we rotated the Bi(111) sample by 180° and measured the spin polarization at six equivalent k points. If the time-reversal symmetry breaks in the initial state of the S_2 state, even after rotating the sample, the larger spin polarization should be observed at points b and f rather than at c and e. Figure 6(b) shows the observed spin polarization at each k point after rotating the Bi(111) sample by 180°. As shown in the inset of Fig. 6 (b), $\phi = 0°$ corresponds to point d, and the order of the measurement positions is d, e, f, a, b, and c. Because of this change of the measurement order, the sign of the out-of-plane spin component becomes the opposite of that before rotation, indicating that the observed sign alternation

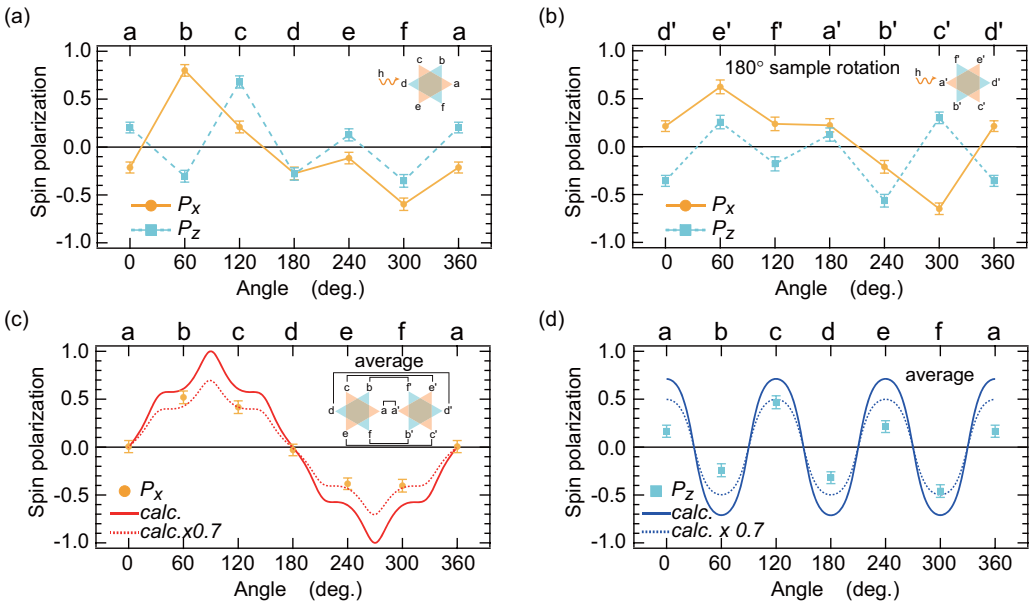

FIG. 6. (a) Azimuth angle ϕ dependence of the in-plane (P_x) and out-of-plane (P_z) spin polarization observed at points a–f in the bottom panel of Fig. 2(c). The angle is defined in the top panel of Fig. 2(c). (b) The same as (a), but after 180° sample rotation around the surface normal. The insets in (a) and (b) indicate each experimental geometry of the measurements. (c) and (d) In-plane and out-of-plane spin polarization obtained by averaging the spin polarization in (a) and (b), respectively. The solid lines represent out-of-plane and in-plane spin polarization calculated by the model Hamiltonian based on the kp theorem.

of the out-of-plane spin component is mainly due to the spin polarization of the initial states of the S_2 state. For the in-plane spin component, even after sample rotation, the spin orientation is still counterclockwise, suggesting that the observed in-plane spin component predominantly reflects the spin texture of the initial state, i.e., the tangential in-plane Rashba spin texture.

Considering the degree of spin polarization, the variation of the in-plane spin polarization again deviates from the curve estimated by the model Hamiltonian [Fig. 6(c)]. That is, the degree of in-plane spin polarization is larger at points e and c than at points f and b after rotation. If the observed magnitude variation of the spin polarization is due to the breaking of the time-reversal symmetry of the initial electronic state as suggested by Takayama and coworkers [23], the degree of spin polarization should be unrelated to the sample rotation; that is, it should be invariably larger at points b and f. However, the observed behavior of the in-plane spin polarization is the other way around, and a high degree of spin polarization is always observed at the k points in the half of the SBZ that is in the light incidence direction, as schematically illustrated in the inset of Fig. 6(b). This result strongly suggests that the observed variation of the in-plane spin polarization at different k points is due to the photoemission final-state effect, which is also supported by the nonzero in-plane spin polarization at points a and d, where no P_x component is expected from the normal helical Rashba spin texture.

Here, to suppress the influence of the final-state effect as much as possible, the spin polarization of the photoelectrons was averaged as shown in Figs. 6(c) and 6(d). As a result, the values of the spin polarization become more symmetric than those before averaging and seem to be closer to the expected initial-state spin polarization. There are two possible reasons for the deviation between the magnitudes of the observed and simulated spin polarizations [Figs. 4(b), 6(c) and 6(d)]: the final-state effect as discussed with regard to Fig. 6 and imperfection of the model Hamiltonian used. Although the magnitude of spin polarization ($|P| = \sqrt{P_x^2 + P_y^2 + P_z^2}$) calculated by the model Hamiltonian is completely 100%, the spin is not always fully polarized in real systems, excluding special cases such as C_3 symmetry [37–40]. Generally, spin-orbit coupling causes intermixing between one spin of even symmetry and the opposite spin of odd symmetry, resulting in reduction of the spin polarization. According to the first-principles calculations in Refs. [41,42], the in-plane spin polarization in the first bilayer is about 70% at $k_x = 0\ \text{Å}^{-1}$ and $k_y = 0.12\ \text{Å}^{-1}$. This estimated spin polarization is comparable to our experimental result at $k_x = 0\ \text{Å}^{-1}$, as shown in Fig. 4(b). A similar tendency of spin-polarization reduction should also be observed in the out-of-plane spin component of Figs. 4(b) and 6(d). Therefore, we multiplied both the in-plane and out-of-plane spin polarizations by a factor of 0.7, and the results are shown as dashed lines in Figs. 6(c) and 6(d). For the in-plane spin component, the calculated spin polarization including the reduction factor is in good agreement with the experimental result. However, for the out-of-plane spin component, results are still inconsistent; that is, the observed spin polarization is still smaller than the calculated spin polarization.

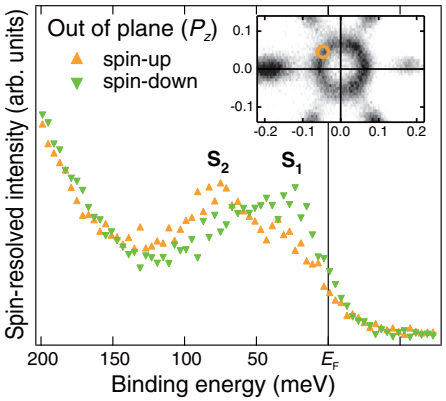

FIG. 7. SARPES spectrum of the out-of-plane spin component P_z taken at the k point indicated by the circles in the FS mapping shown in the inset. Clear out-of-plane spin polarization is observed for the S_1 state (the inner electron pocket). Note that the sign of the spin polarization is opposite that of the S_2 state (the outer petal-like hole pocket).

The inconsistency of the out-of-plane spin polarization can be explained by considering the possible existence of the different domains rotated 180° with respect to the surface normal as reported for a Bi film on the Si(111) surface by x-ray diffraction (XRD) measurements [43]. According to the XRD measurements, the domain population seems to be dependent on the quality of the surface. The highest rate of the domain population is 0.54; that is, the population of the predominant (inferior) domain is 0.77 (0.23). We sometimes observed extinction of the out-of-plane spin polarization at the S_2 state even on the $\bar{\Gamma}$-$\bar{K}$ line [44]. Therefore, the extinction and reduction of the out-of-plane spin polarization in some of the Bi films is probably caused by cancellation of the out-of-plane spin polarization by the two types of domains with opposite spin polarization. By considering this effect, the calculated band structure including spin polarization is in good agreement with the experimental results.

Finally, there is a hexagonal FS in Fig. 2(c), which is reminiscent of the hexagonal warping effect caused by the C_{3v} symmetry in topological insulators typified by Bi_2Te_3. The effect of C_{3v} symmetry is also distinct in the spin texture of the S_1 state. Figure 7 shows the SARPES spectrum of the out-of-plane spin component taken at the k point indicated by the circle in the inner FS (see the inset of Fig. 7), which is along the $\bar{\Gamma}$-$\bar{K}$ line. There is out-of-plane spin polarization. Namely, the spin-down state is dominant at the Fermi level (i.e., the S_1 state). Interestingly, the spin-up state becomes dominant at $E_B \sim 80$ meV, where the S_2 state contributes to the spectrum weight [see Fig. 2(a)]. The opposite signs of spin polarization for S_1 and S_2 are also in agreement with P_z calculated by the model Hamiltonian and a previous first-principles calculation for $Bi_{1-x}Sb_x$ [7]

IV. CONCLUSION

We have investigated the electron spin texture of the surface states (S_1 and S_2) of a Bi(111) film caused by the Rashba spin splitting by means of high-resolution SARPES. In addition

to in-plane spin polarization, a considerable out-of-plane spin component that shows periodic sign reversal of the spin polarization with $2\pi/3$ periodicity is observed in the S_2 state. For the in-plane spin component, although the observed spin feature resembles the spin texture, which was proposed to be symmetry breaking of spin polarization, we have clarified that the different spin polarizations at different k points are caused by the photoemission final-state effect. In the S_1 state, an in-plane spin component with relatively high spin polarization and small but distinct out-of-plane spin polarization are observed. The observed anisotropic band structure and peculiar spin texture of the S_1 and S_2 surface states are well reproduced by the kp model Hamiltonian considering the C_{3v} crystal structure. These findings are important to correctly understand the electronic structure of materials with C_{3v} crystal structure possessing a strong SOI.

ACKNOWLEDGMENTS

This work was partly supported by KAKENHI (Grants No. 19340078 and No. 23244066) and a Grant-in-Aid for Scientific Research (A and B) from the Japan Society for the Promotion of Science. The experiments were performed with the approval of the Proposal Assessing Committee of HSRC (Proposals No. 10-B-14 and No. 11-B-12). The authors are grateful to Prof. E. Krasovskii for fruitful discussions.

[1] L. A. Falkovskii, Sov. Phys. Usp. **11**, 1 (1968).
[2] Y. Fuseya, M. Ogata, and H. Fukuyama, J. Phys. Soc. Jpn. **84**, 012001 (2015).
[3] C. R. Ast, J. Henk, A. Ernst, L. Moreschini, M. C. Falub, D. Pacilé, P. Bruno, K. Kern, and M. Grioni, Phys. Rev. Lett. **98**, 186807 (2007).
[4] K. Sakamoto, H. Kakuta, K. Sugawara, K. Miyamoto, A. Kimura, T. Kuzumaki, N. Ueno, E. Annese, J. Fujii, A. Kodama, T. Shishidou, H. Namatame, M. Taniguchi, T. Sato, T. Takahashi, and T. Oguchi, Phys. Rev. Lett. **103**, 156801 (2009).
[5] S. Hatta, T. Aruga, Y. Ohtsubo, and H. Okuyama, Phys. Rev. B **80**, 113309 (2009).
[6] D. Hsieh, D. Qian, L. Wray, Y. Xia, Y. S. Hor, R. J. Cava, and M. Z. Hasan, Nature (London) **452**, 970 (2008).
[7] H.-J. Zhang, C.-X. Liu, X.-L. Qi, X.-Y. Deng, X. Dai, S.-C. Zhang, and Z. Fang, Phys. Rev. B **80**, 085307 (2009).
[8] Y. Xia, D. Qian, D. Hsieh, L. Wray, A. Pal, H. Lin, A. Bansil, D. Grauer, Y. S. Hor, R. J. Cava, and M. Z. Hasan, Nat. Phys. **5**, 398 (2009).
[9] H. Zhang, C.-X. Liu, X.-L. Qi, X. Dai, Z. Fang, and S.-C. Zhang, Nat. Phys. **5**, 438 (2009).
[10] K. Kuroda, M. Ye, A. Kimura, S. V. Eremeev, E. E. Krasovskii, E. V. Chulkov, Y. Ueda, K. Miyamoto, T. Okuda, K. Shimada, H. Namatame, and M. Taniguchi, Phys. Rev. Lett. **105**, 146801 (2010).
[11] T. Sato, K. Segawa, H. Guo, K. Sugawara, S. Souma, T. Takahashi, and Y. Ando, Phys. Rev. Lett. **105**, 136802 (2010).
[12] K. Kuroda, H. Miyahara, M. Ye, S. V. Eremeev, Y. M. Koroteev, E. E. Krasovskii, E. V. Chulkov, S. Hiramoto, C. Moriyoshi, Y. Kuroiwa, K. Miyamoto, T. Okuda, M. Arita, K. Shimada, H. Namatame, M. Taniguchi, Y. Ueda, and A. Kimura, Phys. Rev. Lett. **108**, 206803 (2012).
[13] T. Arakane, T. Sato, S. Souma, K. Kosaka, K. Nakayama, M. Komatsu, T. Takahashi, Z. Ren, K. Segawa, and Y. Ando, Nat. Commun. **3**, 636 (2012).
[14] M. Neupane, S.-Y. Xu, L. A. Wray, A. Petersen, R. Shankar, N. Alidoust, C. Liu, A. Fedorov, H. Ji, J. M. Allred *et al.*, Phys. Rev. B **85**, 235406 (2012).
[15] K. Miyamoto, A. Kimura, T. Okuda, H. Miyahara, K. Kuroda, H. Namatame, M. Taniguchi, S. V. Eremeev, T. V. Menshchikova, E. V. Chulkov, K. A. Kokh, and O. E. Tereshchenko, Phys. Rev. Lett. **109**, 166802 (2012).
[16] C. R. Ast and H. Höchst, Phys. Rev. Lett. **87**, 177602 (2001).
[17] Y. M. Koroteev, G. Bihlmayer, J. E. Gayone, E. V. Chulkov, S. Blügel, P. M. Echenique, and P. Hofmann, Phys. Rev. Lett. **93**, 046403 (2004).
[18] T. Hirahara, K. Miyamoto, I. Matsuda, T. Kadono, A. Kimura, T. Nagao, G. Bihlmayer, E. V. Chulkov, S. Qiao, K. Shimada, H. Namatame, M. Taniguchi, and S. Hasegawa, Phys. Rev. B **76**, 153305 (2007).
[19] T. Hirahara, K. Miyamoto, A. Kimura, Y. Niinuma, G. Bihlmayer, E. V. Chulkov, T. Nagao, I. Matsuda, S. Qiao, K. Shimada, H. Namatame, M. Taniguchi, and S. Hasegawa, New J. Phys. **10**, 083038 (2008).
[20] Y. Ohtsubo and S. Kimura, New J. Phys. **18**, 123015 (2016).
[21] S. Ito, B. Feng, M. Arita, A. Takayama, R.-Y. Liu, T. Someya, W.-C. Chen, T. Iimori, H. Namatame, M. Taniguchi, C.-M. Cheng, S.-J. Tang, F. Komori, K. Kobayashi, T.-C. Chiang, and I. Matsuda, Phys. Rev. Lett. **117**, 236402 (2016).
[22] M.-Y. Yao, F. Zhu, C. Q. Han, D. D. Guan, C. Liu, D. Qian, and J.-f. Jia, Sci. Rep. **6**, 21326 (2016).
[23] A. Takayama, T. Sato, S. Souma, and T. Takahashi, Phys. Rev. Lett. **106**, 166401 (2011).
[24] T. Okuda, Y. Takeichi, Y. Maeda, A. Harasawa, I. Matsuda, T. Kinoshita, and A. Kakizaki, Rev. Sci. Instrum. **79**, 123117 (2008); T. Okuda, Y. Takeichi, A. Harasawa, I. Matsuda, T. Kinoshita, and A. Kakizaki, Eur. Phys. J. Spec. Top. **169**, 181 (2009).
[25] T. Okuda, K. Miyamaoto, H. Miyahara, K. Kuroda, A. Kimura, H. Namatame, and M. Taniguchi, Rev. Sci. Instrum. **82**, 103302 (2011).
[26] J. Henk, T. Scheunemann, S. V. Halilov, and R. Feder, J. Phys. Condens. Matter **8**, 47 (1996); H. Wortelen, H. Mirhosseini, K. Miyamoto, A. B. Schmidt, J. Henk, and M. Donath, Phys. Rev. B **91**, 115420 (2015).
[27] T. Nagao, J. T. Sadowski, M. Saito, S. Yaginuma, Y. Fujikawa, T. Kogure, T. Ohno, Y. Hasegawa, S. Hasegawa, and T. Sakurai, Phys. Rev. Lett. **93**, 105501 (2004).
[28] S. Yaginuma, T. Nagao, J. T. Sadowski, A. Pucci, Y. Fujikawa, and T. Sakurai, Surf. Sci. **547**, L877 (2003).
[29] F. Reinert, G. Nicolay, S. Schmidt, D. Ehm, and S. Hüfner, Phys. Rev. B **63**, 115415 (2001).
[30] L. Fu, Phys. Rev. Lett. **103**, 266801 (2009).
[31] S. Souma, K. Kosaka, T. Sato, M. Komatsu, A. Takayama, T. Takahashi, M. Kriener, K. Segawa, and Y. Ando, Phys. Rev. Lett. **106**, 216803 (2011).

[32] F. Meier, H. Dil, J. Lobo-Checa, L. Patthey, and J. Osterwalder, Phys. Rev. B **77**, 165431 (2008).
[33] E. Frantzeskakis and M. Grioni, Phys. Rev. B **84**, 155453 (2011).
[34] S. Vajna, E. Simon, A. Szilva, K. Palotas, B. Ujfalussy, and L. Szunyogh, Phys. Rev. B **85**, 075404 (2012).
[35] K. Miyamoto, A. Kimura, T. Okuda, K. Shimada, H. Iwasawa, H. Hayashi, H. Namatame, M. Taniguchi, and M. Donath, Phys. Rev. B **86**, 161411(R) (2012).
[36] S. D. Stolwijk, K. Sakamoto, A. B. Schmidt, P. Krüger, and M. Donath, Phys. Rev. B **91**, 245420 (2015).
[37] C.-X. Liu, X.-L. Qi, H. J. Zhang, X. Dai, Z. Fang, and S.-C. Zhang, Phys. Rev. B **82**, 045122 (2010).
[38] K. Miyamoto, H. Wortelen, H. Mirhosseini, T. Okuda, A. Kimura, H. Iwasawa, K. Shimada, J. Henk, and M. Donath, Phys. Rev. B **93**, 161403(R) (2016).
[39] K. Sakamoto, T. Oda, A. Kimura, K. Miyamoto, M. Tsujikawa, A. Imai, N. Ueno, H. Namatame, M. Taniguchi, P. E. J. Eriksson, and R. I. G. Uhrberg, Phys. Rev. Lett. **102**, 096805 (2009).
[40] K. Yaji, K. Kuroda, S. Toyohisa, A. Harasawa, Y. Ishida, S. Watanabe, C. Chen, K. Kobayashi, F. Komori, and S. Shin, Nat. Commun. **8**, 14588 (2017).
[41] A. Kimura, E. E. Krasovskii, R. Nishimura, K. Miyamoto, T. Kadono, K. Kanomaru, E. V. Chulkov, G. Bihlmayer, K. Shimada, H. Namatame, and M. Taniguchi, Phys. Rev. Lett. **105**, 076804 (2010).
[42] E. Krasovski (private communication).
[43] T. Shirasawa, M. Ohyama, W. Voegeli, and T. Takahashi, Phys. Rev. B **84**, 075411 (2011).
[44] H. Miyahara, T. Maegawa, K. Kuroda, A. Kimura, K. Miyamoto, H. Namatame, M. Taniguchi, and T. Okuda, e-J. Surf. Sci. Nanotechnol. **10**, 153 (2012).